

Glacial-Interglacial Atmospheric CO₂ Change —The Glacial Burial Hypothesis

Ning ZENG*

Department of Meteorology and Earth System Science Interdisciplinary Center, University of Maryland, USA

(Received 22 January 2003; revised 29 April 2003)

ABSTRACT

Organic carbon buried under the great ice sheets of the Northern Hemisphere is suggested to be the missing link in the atmospheric CO₂ change over the glacial-interglacial cycles. At glaciation, the advancement of continental ice sheets buries vegetation and soil carbon accumulated during warmer periods. At deglaciation, this burial carbon is released back into the atmosphere. In a simulation over two glacial-interglacial cycles using a synchronously coupled atmosphere-land-ocean carbon model forced by reconstructed climate change, it is found that there is a 547-Gt terrestrial carbon release from glacial maximum to interglacial, resulting in a 60-Gt (about 30-ppmv) increase in the atmospheric CO₂, with the remainder absorbed by the ocean in a scenario in which ocean acts as a passive buffer. This is in contrast to previous estimates of a land uptake at deglaciation. This carbon source originates from glacial burial, continental shelf, and other land areas in response to changes in ice cover, sea level, and climate. The input of light isotope enriched terrestrial carbon causes atmospheric $\delta^{13}\text{C}$ to drop by about 0.3‰ at deglaciation, followed by a rapid rise towards a high interglacial value in response to oceanic warming and regrowth on land. Together with other ocean based mechanisms such as change in ocean temperature, the glacial burial hypothesis may offer a full explanation of the observed 80–100-ppmv atmospheric CO₂ change.

Key words: atmospheric CO₂, ice age, glacial burial hypothesis, climate

1. Introduction

Atmospheric CO₂ concentration has varied throughout Earth's history, often in synchrony with temperature and other climate variables. Measure-

ments of air trapped in Antarctica ice cores have revealed large CO₂ variations over the last four 100-kyr (thousands of years) glacial-interglacial cycles, in particular, the 80–100 ppmv increase from glacial maxima to interglacials (Petit et al., 1999; Fig. 1).

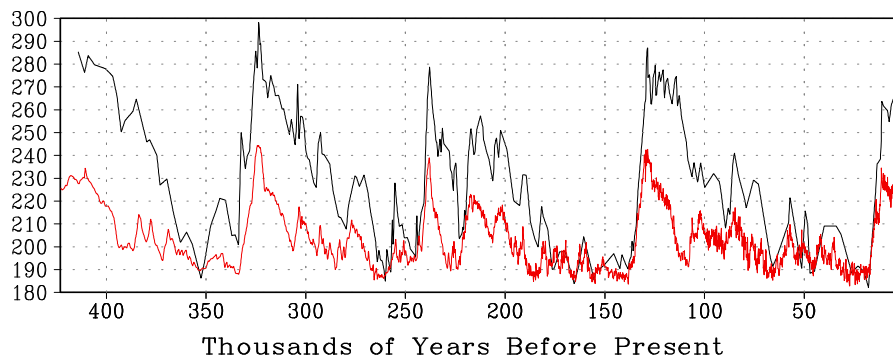


Fig. 1. History of atmospheric CO₂ (black line, in ppmv) and temperature (red, in relative units) over the last 420,000 years from the Vostok ice core; after Petit et al. (1999)

*E-mail: zeng@atmos.umd.edu; <http://www.atmos.umd.edu/~zeng>

Table 1. Estimates of the difference of carbon stored on land between the Holocene and the last glacial maximum using various methods (in Gt; Holocene minus LGM: positive value indicates larger storage at the Holocene). The sources are grouped into three categories according to the method used: marine ^{13}C inference (with the $\delta^{13}\text{C}$ value listed), paleoecological data, and biosphere model forced by reconstructed climate (with the climate model and biosphere model listed). Modified from Maslin and Thomas (2003)

Source	Method	Land carbon difference (Holocene–LGM)
Shackleton, 1977	ocean $\delta^{13}\text{C}$, 0.7‰	1000
Berger and Vincent, 1986	ocean $\delta^{13}\text{C}$, 0.40‰	570
Curry et al., 1988	ocean $\delta^{13}\text{C}$, 0.46‰	650
Duplessy et al., 1988	ocean $\delta^{13}\text{C}$, 0.32‰	450
Broecker and Peng, 1993	ocean $\delta^{13}\text{C}$, 0.35‰	425
Bird et al., 1994	ocean $\delta^{13}\text{C}$	270–720
Maslin et al., 1995	ocean $\delta^{13}\text{C}$ 0.40+0.14‰	400–1000 (700)
Beerling, 1999	^{13}C inventory	550–680
Adams et al., 1990	palaeoecological data	1350
Van Campo et al., 1993	palaeoecological data	430–930 (713)
Crowley, 1995	palaeoecological data	750–1050
Adams and Faure, 1998	palaeoecological data	900–1900 (1500)
Prentice and Fung, 1990	GISS, Holdridge/C Density	-30 to 50
Friedlingstein et al., 1992	Sellers, SLAVE	300
Prentice et al., 1993	ECMWF T21, BIOME	300–700
Esser and Lautenschlager., 1994	ECHAM, HRBM	-213 to 460
Friedlingstein et al., 1995	GISS/Sellers, SLAVE	507–717 (612)
Peng et al., 1995	Pollen Recon., OBM	470–1014
Francois et al., 1998	ECHAM2, CARAIB	134–606
Beerling, 1999	UGAMP/NCAR, SDGVM	535–801 (668)
Otto et al., 2002	4 PMIP models, CARAIB	828–1106
Kaplan et al., 2002	UM, LPJ	821
This study	CCM1, VEGAS	-395 to -749 (-547)

Numerous attempts have been made over the last two decades to explain the lower atmospheric CO_2 at glacial times. Nearly all hypotheses rely on mechanisms of oceanic origin, such as changes in ocean temperature and salinity, reorganization of the thermohaline circulation, changes in carbonate chemistry, enhanced biological pump due to dust fertilization, and effects of sea ice changes (Martin, 1990; Broecker and Henderson, 1998; Sigman and Boyle, 2000; Archer et al., 2000; Falkowski et al., 2000; Stephens and Keeling, 2000; Gildor and Tziperman, 2001), but there is no widely accepted scenario. Attempts in combining these processes also fall short of explaining the full range and amplitude of observational constraints (Ridgwell, 2001).

Part of the difficulty is that besides the change in the atmospheric carbon pool, these ocean based theories also have to accommodate additional carbon from the terrestrial biosphere which is generally thought to have lower carbon storage at glacial times. Estimates of terrestrial carbon difference between the

Holocene and the last glacial maximum (LGM) range from -213 to 1900 Gt (Gigaton or 10^{15}g), with pollen-based paleoecologically reconstructed estimates often larger than marine carbon 13 inference and terrestrial carbon model results (Shackleton, 1977; Adams et al., 1990; Prentice and Fung, 1990; Crowley, 1995; and Table 1). A typical partitioning of glacial to interglacial carbon cycle change is a 170-Gt increase in the atmosphere, a 500-Gt increase on land, and a 670-Gt decrease in the ocean and sediments (e.g., Sundquist, 1993; Sigman and Boyle, 2000).

The terrestrial biosphere has been thought to store less carbon at glacial times because the drier, colder, and low CO_2 glacial climate is less favorable for vegetation growth. In addition, at glacial maximum, large areas in the Northern Hemisphere are covered under ice, thus it is supposed that less land is available for carbon storage, which is partially compensated for by carbon accumulation on raised continental shelves due

to lower glacial sea level.

2. The glacial burial hypothesis

However, looking at the glacial-interglacial cycle as an evolving phenomenon, a question naturally arises (Olson et al., 1985): if no carbon was present under the ice sheets at a glacial maximum, what happened to the carbon accumulated in those areas during the preceding interglacial? The consideration of the fate of this carbon pool has led to the proposal that glacial burial carbon is the missing link in the glacial CO₂ problem. A rudimentary version of the hypothesis follows.

At interglacial time, the organic carbon stored in the terrestrial biosphere is about 2100 Gt, of which approximately 600 Gt is distributed in the vegetation biomass of leaf, root, and wood, and the other 1500 Gt is stored as soil carbon (Schlesinger, 1991). While vegetation carbon is mainly in the tropical and temperate forests, soil carbon tends to concentrate in middle and high latitude cold regions, because of the slow decomposition rate there.

As the glacial condition sets in, vegetation and soil carbon gets covered under ice, and thus insulated from contact with the atmosphere. Given the present carbon distribution and the ice cover distribution at the last glacial maximum, the amount of carbon that would have been covered under ice is estimated about 500 Gt.

At deglaciation, this glacial burial carbon is exposed to the atmosphere again, and subsequently decomposed and released into the atmosphere, thus contributing to the observed increase in atmospheric CO₂. The sequence of events at the stages of a full glacial-interglacial cycle are depicted in Fig. 2.

If the 500 Gt of carbon from land were released into the atmosphere overnight, it would lead to an increase of atmospheric CO₂ concentration of 250 ppmv, more than a doubling of the glacial CO₂ value. This potential cannot be realized because most of this carbon would have been absorbed by the ocean. The excessive carbon would have been lowered by half in less than 10 years as it gets into the upper ocean, and further lowered to 45 ppmv in about 1000 years due to deep ocean mixing. A further reduction to 15 ppmv on the timescale of 5-10 kyr would result from ocean sediment dissolution (Sigman and Boyle, 2000).

Additional factors can slow down the increase in atmospheric CO₂. First, the retreat of ice sheets takes place on a timescale of 10 000 years because the negative feedback placed on temperature to melt ice. Thus the release of terrestrial carbon is a relatively slow process. Secondly, as ice sheets retreat,

vegetation regrowth takes place via primary and secondary successions, acting as a carbon sink for the atmosphere. However, regrowth is slowed by the speed of seed dispersal, and more importantly, by soil development which can take thousands of years or longer to go from bare rock to being able to support boreal forests. For instance, some northern soil has not reached equilibrium since the retreat of the Laurentide Ice Sheet (Harden et al., 1992).

The details of glaciation history are not well known. An alternative hypothesis about the fate of glacial burial carbon is that as ice sheets advance,

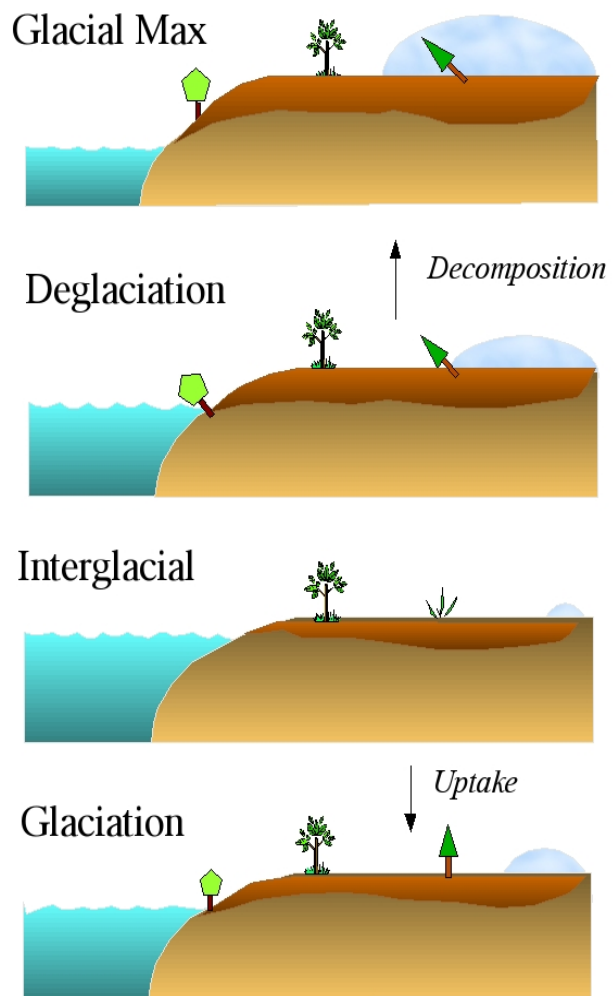


Fig. 2. Illustration of the glacial burial hypothesis and the changes in terrestrial carbon pools over the stages of a glacial-interglacial cycle. Arrows indicate the direction of land-atmospheric carbon flux; reddish brown represents soil carbon; green trees represent vegetation carbon. Land carbon accumulated during glaciation due to glacial advance, sea level lowering, and climate change is released into the atmosphere at the ensuing deglaciation, contributing to the increase in atmospheric CO₂. The ocean damps the land flux, in addition to other active changes such as ocean temperature change.

vegetation and soil organic matter is disturbed and decomposed at an early stage, therefore little carbon is buried under the ice sheets at glacial maximum. While one cannot exclude this mechanism in destroying some carbon, especially the episodically fast-moving ice streams at the front range of a mature ice sheet (MacAyeal, 1993), this 'bulldozer' scenario is unlikely during continental-scale ice sheet inception because ice sheet movement becomes significant only at large thickness. Instead, the terrestrial carbon is cooled and buried slowly after the point when summer heating fails to melt away winter snow. The bottom line is that, regardless of the exact timing of the decomposition, terrestrial carbon needs to be accounted for in the regions where ice sheets come and go.

In summary, the deglaciation atmospheric CO₂ increase depends on the interplay of a number of mechanisms on multiple timescales in a transient fashion. After ocean uptake, land carbon release alone may contribute somewhere between 15 and 45 ppmv to the atmospheric CO₂ increase, thus paving the way for explaining the remaining CO₂ increase by other ocean based mechanisms.

Besides the need for including glacial burial carbon and delayed regrowth, recent progress in terrestrial carbon research also demands a reassessment of the climate sensitivity of the terrestrial biosphere. For instance, the reduced productivity due to lower glacial CO₂ level may not be as strong as represented in many models as the CO₂ fertilization effect may have been overestimated on a global scale (Field, 2001). The generally colder glacial climate would have decreased soil respiration loss without necessarily increasing vegetation biomass or changing vegetation types, thus leaving more carbon on land. This is an important process not accounted for by paleoecological estimates and some models. On the other hand, colder and drier climate leads to less favorable growing conditions in high mountains and the arctic regions. These competing effects need to be addressed quantitatively.

Research in the past has typically viewed the glacial CO₂ problem as a static problem with two near-equilibrium states: glacial and interglacial. The current theory emphasizes its time-dependent nature. Of particular importance are: the burial and delayed release of terrestrial carbon by ice sheets; the change of vegetation and soil carbon as climate and sea level change during the glacial-interglacial cycles; and the capacity and multiple timescales in ocean and sediment chemistry in buffering atmospheric CO₂, as well as other active oceanic mechanisms. These details are studied in a global carbon cycle model with a focus on

the 100-kyr cycle.

3. A coupled atmosphere-land-ocean carbon model

Since the atmospheric mixing time is much shorter than the glacial timescales, a box atmosphere carbon model is used to couple the terrestrial and ocean carbon models (see Appendix). In the coupled system, the terrestrial carbon influences ocean and atmosphere in that any imbalance in the land carbon budget is released into the atmosphere and the change in atmospheric CO₂ partial pressure then causes ocean and sediment adjustment.

As a basis for understanding the time evolution over glacial-interglacial cycles, Fig. 3 shows the climatology simulated by the terrestrial carbon model at equilibrium interglacial. The Net Primary Production (NPP) and vegetation carbon (wood, root, and leaf) are dominated by tropical, temperate, and boreal forests, largely in accordance with precipitation distribution and low maintenance requirement at colder regions. However, soil carbon is smaller in the tropics than at high latitudes because of the fast decomposition at high temperature in the tropics. As a result, the total carbon (vegetation+soil) per unit area has similar magnitude at tropical and high latitude moist regions, but northern mid-high latitudes dominate the total budget because of the large continental area. The global land total carbon pool is 1651 Gt, with 903 Gt in the soil and 748 Gt in the vegetation biomass. These are within the uncertainties of estimates of the present-day carbon budget (Schlesinger, 1991). It is not entirely satisfactory to use modern climate and carbon pool size for the interglacial period, but the relatively small variations within an interglacial period such as the Holocene period are not scrutinized here because the goal is to explain the much larger glacial-interglacial CO₂ change also applicable to earlier glacial cycles. Also note that this equilibrium interglacial is not the same as the transient interglacial discussed below.

To simulate the time-dependent glacial-interglacial cycles, the terrestrial carbon model is forced by the following climate boundary conditions during deglaciation: ice cover and topography from 21 to 6 kBP (thousands of years before present) at 1-kyr intervals (Peltier, 1994), and simulated climate (precipitation and surface temperature) of the NCAR Community Climate Model (CCM1) (Kutzbach et al., 1998) for the time slices 21, 16, 14, 11, and 6 kBP. In order to avoid bias in the CCM1 simulation, anomalies for precipitation and temperature are computed relative to its control simulation. These anomalies are then added to a

modern observed climatology (New et al., 1999) to obtain the full values. The ice data are linearly interpolated at a time interval of 10 years while precipitation and temperature are interpolated monthly. To better represent the carbon fertilization effect, the CO_2 used in the vegetation photosynthesis module (CO2v) takes a value of 200 ppmv at glacial maximum and 280 ppmv at the interglacial with linear interpolation in between. Otherwise, using the modeled CO_2 would add unnecessary uncertainty. The terrestrial model was run at $2.5^\circ \times 2.5^\circ$ horizontal resolution at a monthly time step to resolve the seasonal cycle.

The details of ice sheet inception and climate change during glaciation are not well constrained. Precipitation, temperature, and CO2v were simply inter-

polated linearly using the data of the Holocene maximum (6 kBP) and the LGM (21 kBP), because the focus here is the 100 kyr cycle, not the sub-100-kyr variations. An ‘inverse deglaciation’ technique is used for the ice data such that a place with earlier (later) deglaciation would glacialate later (earlier). The averages of these forcings over land are shown in Fig. 4a, b.

The ocean carbon model was forced by interglacial oceanic circulation, temperature, and salinity. These conditions stay fixed throughout the model run (except for a sensitivity experiment) so ocean acts as a passive buffer because the focus here is on land. The ocean model was run at a yearly time step.

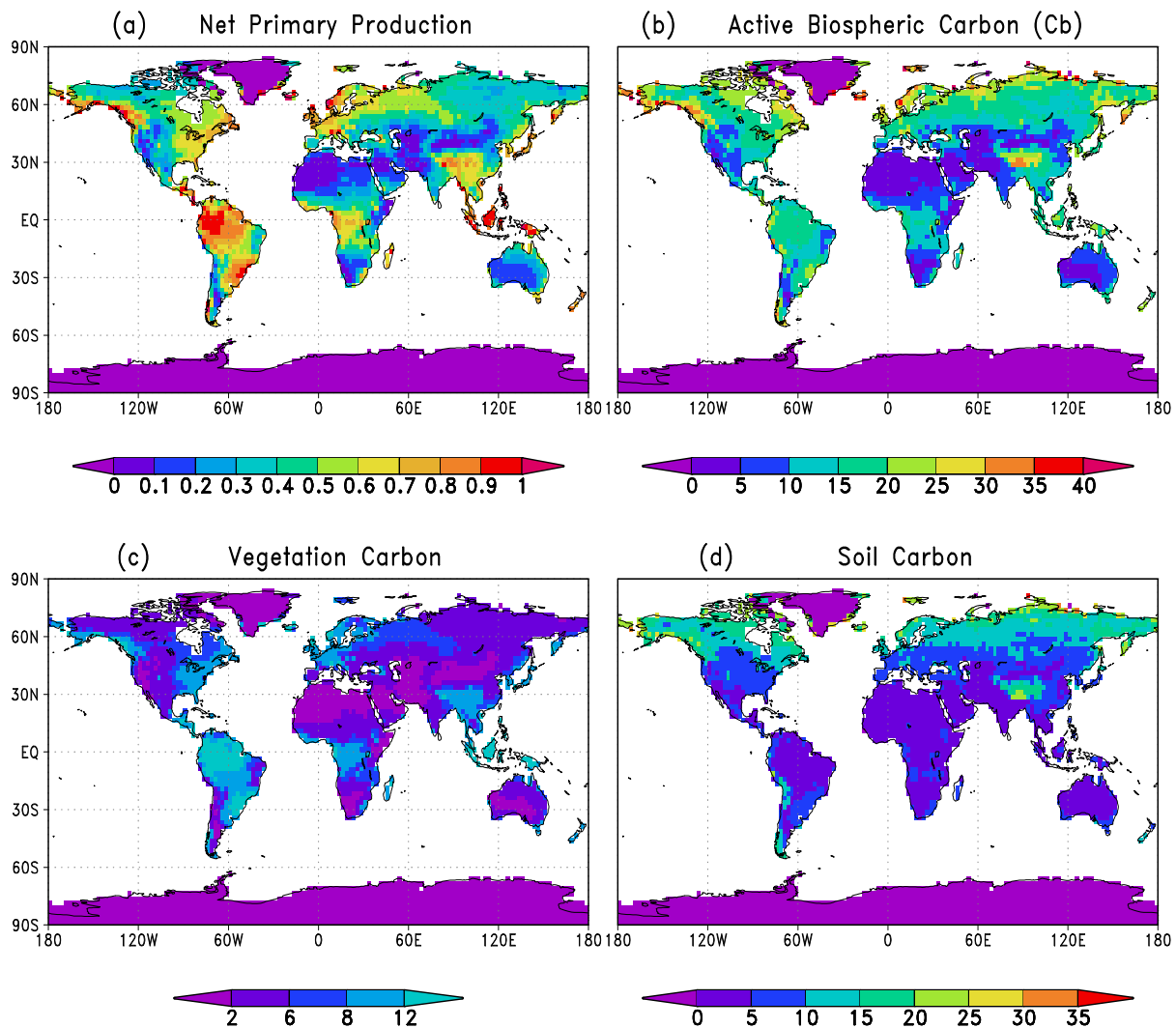


Fig. 3. Model simulated land Net Primary Production NPP ($\text{kg m}^{-2} \text{yr}^{-1}$) and carbon pools (kg m^{-2}) for equilibrium interglacial condition (not identical to a transient interglacial which includes glacial burial carbon decomposition and regrowth uptake).

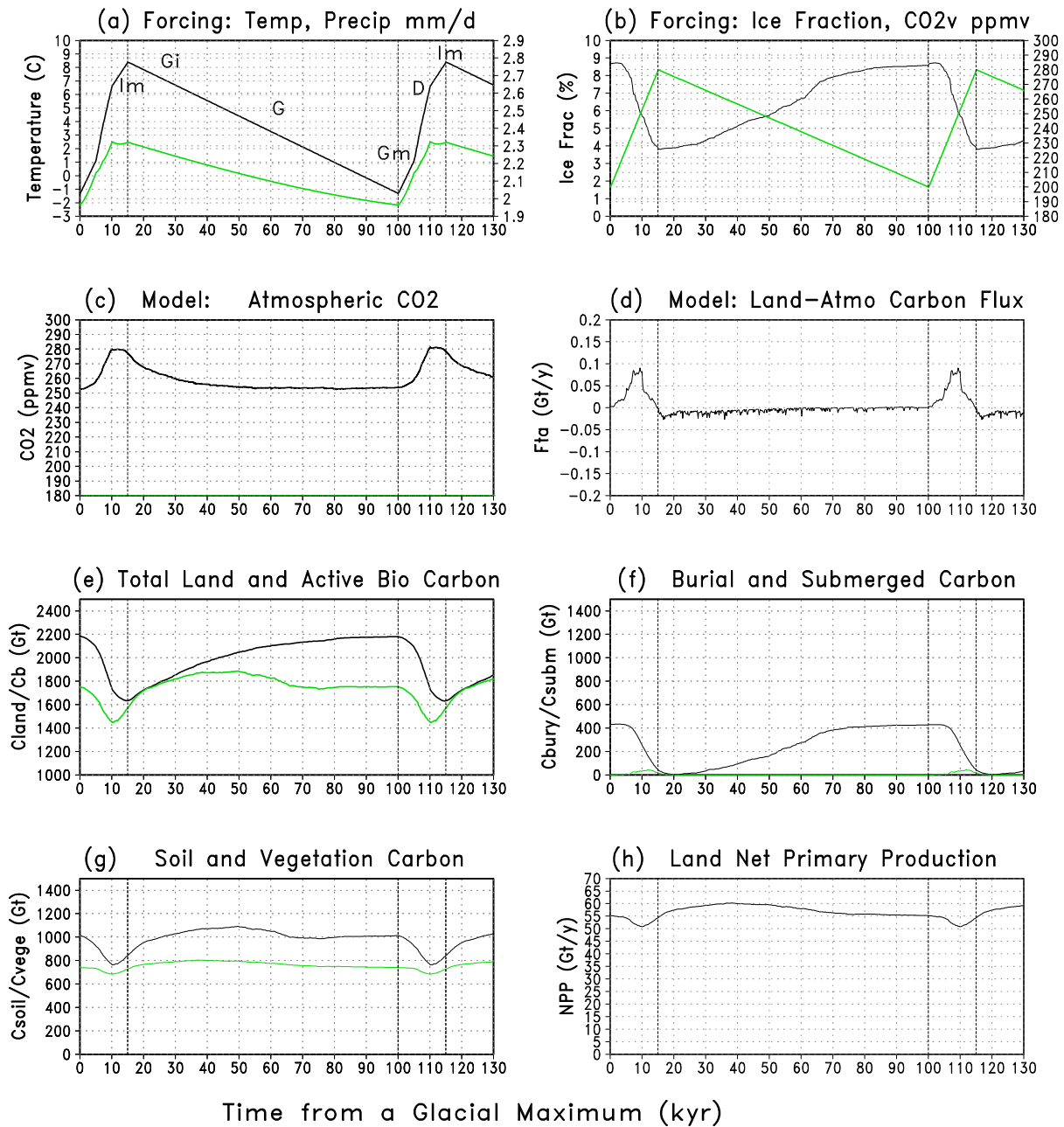


Fig. 4. Climate forcings (a-b) and model simulation (c-h) over glacial-interglacial cycles: (a) Temperature (black line, labeled on the left in Celsius) and precipitation (green, labeled on the right in mm d^{-1}) averaged over land; (b) Ice covered area as percentage of world total (black), CO₂ used in vegetation photosynthesis (green); (c) Simulated atmospheric CO₂ concentration; (d) Net carbon flux from land to atmosphere; (e) Total land (black) and active biospheric (green) carbon; (f) Glacial burial carbon (black) and submerged carbon on continental shelves at rising sea level (green); (g) Carbon stored in soil (black) and vegetation biomass (green); (h) Net primary production. Vertical lines mark two interglacials (year 15k, 115k) and a glacial maximum (year 100k). Labeled in (a) are the different stages of a GI cycle defined in the text. An increase of 30 ppmv atmospheric CO₂ at deglaciation (c) is the direct result of about 500 Gt carbon released from land (e) in a scenario in which ocean acts only as a passive buffer.

4. Glacial-interglacial cycle as a transient phenomenon

The coupled model forced by the above climate boundary conditions is first brought to an interglacial equilibrium for 5 kyr. It then runs through two glaciation-deglaciation cycles, plus an additional 15 kyr of glaciation. Each glaciation lasts 85 kyr while it takes 15 kyr for deglaciation, corresponding to the 21–6 kBP boundary data. Thus the total run time is 220 kyr. The results for the last 130 kyr are shown in Fig. 4 c–h. For the convenience of interpretation, the important stages of a glacial-interglacial cycle (GI cycle) are referred to as: Im—Interglacial, Gi—Glacial Inception, G—Glaciation, Gm—Glacial Maximum, D—Deglaciation.

The climate forcings in Fig. 4a and 4b show that from interglacial Im to glacial maximum Gm, the global mean land temperature is lower by 9°C, precipitation by 0.3 mm d⁻¹. The ice-covered area drops from 9% to 4% of the total world area (500 million km²), corresponding to the wax and wane of the ice sheets.

The modeled atmospheric CO₂ (Fig. 4c) shows a relatively rapid decrease at early glaciation (Gi), followed by a slow decline toward a minimum of about 250 ppmv at Gm. The deglaciation CO₂ increase starts slowly but rises rapidly to 280 ppmv between 5–10 kyr after Gm. It then levels off before the next glaciation drives down the CO₂ level again. The change of atmospheric CO₂ during a GI cycle is about 30 ppmv.

The rise and fall in atmospheric CO₂ is a direct response to land-atmosphere carbon exchange, with ocean playing an important buffering role. The net carbon flux from land to atmosphere F_{ta} [or Net Biome Exchange (NBE), including the Net Ecosystem Exchange (NEE) of the active biosphere, as well as the respiration of exposed burial carbon and submerged continental shelf carbon at deglaciation] is negative throughout the glaciation period with a value of -0.02 Gt yr⁻¹ for the first 10 kyr. Carbon is released rapidly during deglaciation at a peak rate of 0.1 Gt yr⁻¹ (Fig. 4d). The small but fast changes (wiggles) in F_{ta} are numerical artifacts due to the decomposition of suddenly re-exposed ice-buried grid points and water-covered continental shelf points, rather than fast climate change which the model does not attempt to simulate, and it has no cumulative impact on the results.

The net land-atmosphere carbon flux F_{ta} is the result of the change in total land carbon storage such that $\Delta C_{\text{land}} = -\int F_{ta} dt$, where t is time. A total of

547 Gt (Fig. 4e) is assimilated on land from interglacial to glacial maximum which is released into the atmosphere at deglaciation, leading to a 60 Gt (about 30 ppmv) increase in atmospheric CO₂, with the rest absorbed by the ocean. Thus the crucial question is what caused such a large change in land carbon storage?

The land carbon consists of three reservoirs:

$$C_{\text{land}} = C_{\text{b}} + C_{\text{bury}} + C_{\text{subm}}, \quad (1)$$

where $C_{\text{b}} = C_{\text{vege}} + C_{\text{soil}}$ is the active terrestrial biosphere (with active growth in vegetation) carbon including vegetation and soil carbon, C_{bury} is the dead organic carbon buried under ice at glacial times, and C_{subm} is the continental shelf carbon submerged under water when sea level rises.

During glaciation, ice sheets advance, covering both vegetation and soil carbon present at the site. The burial is modeled as an instantaneous process as soon as ice covers the location and the buried carbon is removed from C_{b} and lumped into one reservoir C_{bury} and subsequently insulated from exchange with the atmosphere. Before burial, their growth and respiration are subject to the climate forcing with the seasonal cycle like other places. When reexposed at the next deglaciation, they are treated like the slow soil carbon pool with a decomposition timescale of 1000 years at 25°C. The change in this reservoir therefore follows the ice coverage closely, and increases from 46 Gt at the interglacial to 427 Gt at glacial maximum, a 381-Gt change (Fig. 4f and Table 2). The nonzeroness at Im is due to the incomplete decomposition of freshly exposed burial carbon. The glacial burial carbon is distributed over an area of about 23×10^6 m² where ice cover changes from Gm to Im.

The active biospheric carbon C_{b} (Fig. 4e) increases rapidly at late deglaciation and early glaciation (years 110 k–120 k) by about 300 Gt, as a result of the delayed regrowth on the previously ice-covered area. This delay mimics the time required for soil development and seed dispersal. The modeled soil development depends on the rate of vegetation-to-soil turnover (fallen leaves, dead roots, and wood) and it is typically 2–3 kyr up to 5 kyr at regions with low productivity. Photosynthesis is limited by soil development before it reaches a predefined depth of 1 meter. Thus NPP (Fig. 4h) and C_{b} have a similar delayed increase, followed by a slower increase in response to climate change (years 20 k–50 k). Both then drop off due to ice sheet advancement claiming land previously occupied by the active biosphere reservoir C_{b} . This is of course accompanied by an increase in the burial carbon, therefore the total land carbon C_{land} continues to increase throughout glaciation.

Table 2. Carbon pools on land at Interglacial (Im), Glacial Maximum (Gm), and the difference (Gm-Im; note the sign difference from Table 1)

Carbon Pools (Gt)	Symbol	Interglacial	Glacial Max	Gm-Im
Total Land	C_{land}	1633	2180	547
Active Biosphere	C_b	1568	1753	185
Glacial Burial	C_{bury}	46	427	381
Submerged on Shelf	C_{subm}	19	0	-19
Vegetation	C_{vege}	727	741	14
Soil	C_{soil}	841	1012	171
Area changing ice	C_{ice}	315	431	116
Continental Shelf	C_{shelf}	21	254	233
Non-ice/shelf	C_{nois}	1297	1495	198
Non-Shelf	$C_{nonshelf}$	1566	1499	-67

Difference of Glacial Max and Interglacial (Gm-Im)

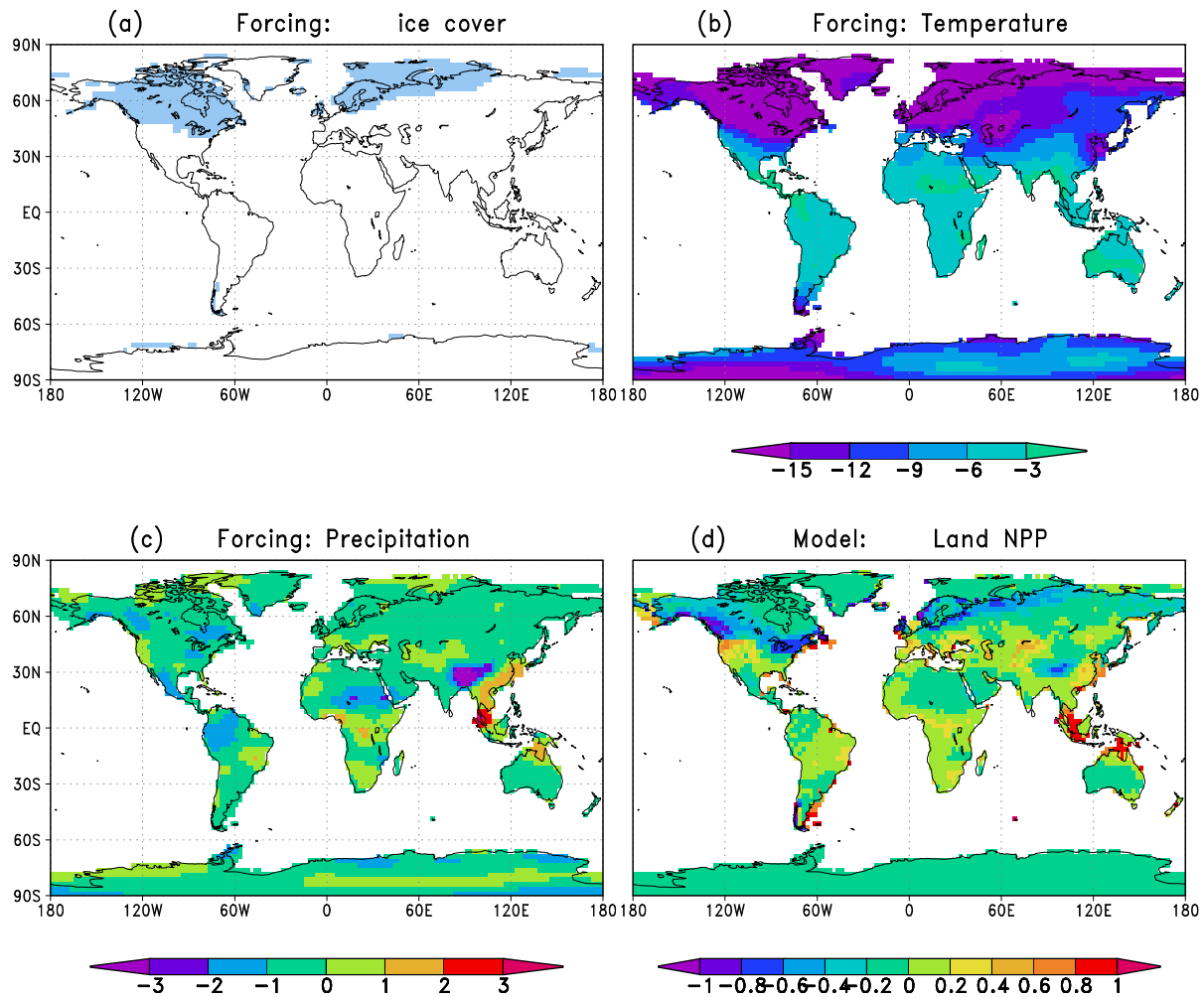


Fig. 5. Differences between glacial maximum (Gm, year 100 k) and interglacial (Im; year 115 k) with forcings in (a)-(c), and simulation in (d)-(j). (a) ice cover (0 or 1); (b) Land temperature (Celsius); (c) Precipitation (mm d^{-1}); (d) Net primary production ($\text{kg m}^{-2} \text{y}^{-1}$).

Difference in Carbon Pools (Gm-Im)

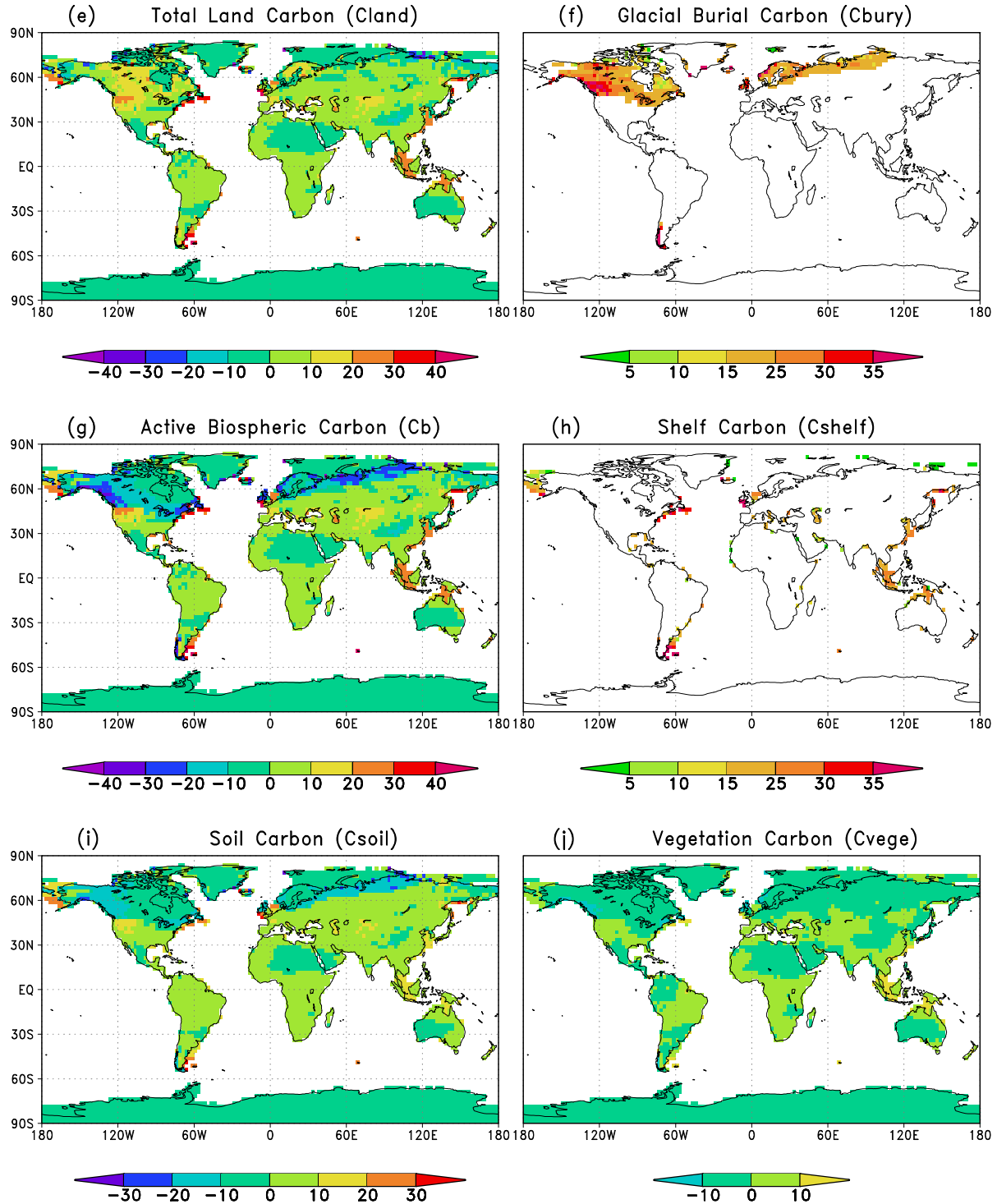


Fig. 5. Continued. Difference in model carbon pools ($Gm-Im$, in $kg\ m^{-2}$) of (e) Total land carbon storage; (f) Glacial burial carbon; (g) Carbon in area with active vegetation growth; (h) Carbon on continental shelves not covered by ice; (i) Soil carbon; (j) Vegetation carbon. The larger carbon storage at glacial maximum is due to a combination of changes in glacial burial, continental shelf, and active biospheric carbon.

The change in active biospheric carbon C_b is dominated by the soil carbon pool (Fig. 4g), because of its large size in the boreal region with ice burial. Even excluding the burial region, the smaller vegetation carbon change is the result of two countering effects: the lowering of CO_2 which leads to lower productivity, and the lowering of respiration due to lower temperature which leads to less carbon loss. The submerged carbon pool C_{subm} (Fig. 4f) is small at any given time because the pool size is zero at Gm (shelf carbon is part of C_b at Gm), and decomposition starts as soon as it is submerged under water. But its cumulative contribution to deglacial CO_2 is significant because total shelf carbon change is 233 Gt (Table 2).

5. Land carbon change

This model predicts a 547-Gt larger land carbon storage during glacial maximum than interglacial, thus land acts as a carbon source during a glacial-interglacial transition, contrary to the widely-held view that the terrestrial biosphere acts as a net sink to the atmosphere (Table 1). It is thus crucially important to understand this difference.

Figure 5 shows the glacial-interglacial difference in land carbon and its partitioning into sub-reservoirs, as well as the difference in climate forcing. The most dramatic difference is the ice cover change related to the waxing and waning of the Northern Hemisphere ice sheets such as the Laurentide and Fennoscandian ice sheets. Part of the raised continental shelf area at Gm can be inferred from Fig. 5h (only non-ice covered shelf area is shown). The glacial precipitation is drier in many regions of the world, in particular, the areas covered by the ice sheets and surrounding regions such as Siberia and North America, as well as large areas of the subtropical dry zones. Noticeable exceptions include central Africa, southeastern Asia, and the western United States. The wetting and cooling of the American west is due to a southward deflection of the jetstream, and is supported by observations such as the existence of the large ancient Lake Bonneville. The surface temperature is 3–15°C cooler in most non-ice covered continental regions. Thus the conventional wisdom of a drier and colder glacial climate is true for temperature (global land mean of 9°C, but about half if ice covered regions are excluded), but only partially true for precipitation (global land mean of only 0.3 mm d⁻¹ drier) according to the CCM1 simulation. This not so dry but much colder condition contributes a fraction of the difference in carbon storage found in the current study.

The net primary production (Fig. 5d) is higher at Gm in these wetter areas which expand slightly into

the surrounding regions as lower temperature reduces plant respiration loss. As a result, vegetation carbon shows a similar pattern (Fig. 5j). This expansion of higher carbon storage area further extends outward for soil carbon (Fig. 5i) such that most of the areas not covered by ice have slightly higher carbon storage at glacial maximum (Fig. 5g). Adding the burial, active biospheric and submerged carbon together, the total land carbon C_{land} (Fig. 5e) shows a predominantly higher carbon storage at Gm in most land areas, causing the 547-Gt difference.

To further understand the regional differences, Fig. 6 shows the time series of a few representative locations. At Ontario, vegetation grows and carbon is stored at late deglaciation (year 11 k) and then freezes at 25 kg m⁻² when covered under the Laurentide Ice Sheet (year 48 k), which is not released back into the atmosphere until the next deglaciation (year 111 k). The otherwise rapid initial growth is slowed down somewhat by soil development. This delayed regrowth results in a dip in C_{land} of about 13 kg m⁻² shortly before 1m, which leads to a net glacial burial release of 12 kg m⁻² (25 minus 13) into the atmosphere. This release would be 25 kg m⁻² if the regrowth delay is 5 kyr or longer so the burial carbon can decompose completely beforehand. On the other hand, if there were no regrowth delay at all, the limiting timescale would be that of the slow soil carbon pool, leading to a smaller net land carbon release. This demonstrates the subtle interplay among different timescales of different processes and the importance of considering the GI cycle as a transient phenomenon.

In front of the Laurentide Ice Sheet (Maryland) and at a tropical rainforest site (Amazon), the controlling factors are the forcing temperature, precipitation, and CO_2 . Both sites show very little variation compared to the dramatic change at Ontario, largely due to the countering effects of CO_2 and temperature. At the land bridge linking New Guinea and Australia (termed ‘Old Guinea’), vegetation growth and carbon accumulation is fast at year 54 k because, unlike the ice covered region, no soil development is assumed to be required there. This shelf carbon is submerged at year 108 k (it turns from the active biospheric pool C_b into the submerged pool C_{subm} in this paper’s bookkeeping approach), and is completely decomposed within 3000 years.

It is illuminating to partition the global total land carbon according to the characteristic areas constant in time as (Fig. 7):

$$C_{\text{land}} = C_{\text{ice}} + C_{\text{shelf}} + C_{\text{nois}} , \quad (2)$$

where C_{ice} is the carbon in the areas where ice sheets wax and wane during GI cycles, C_{shelf} is the carbon

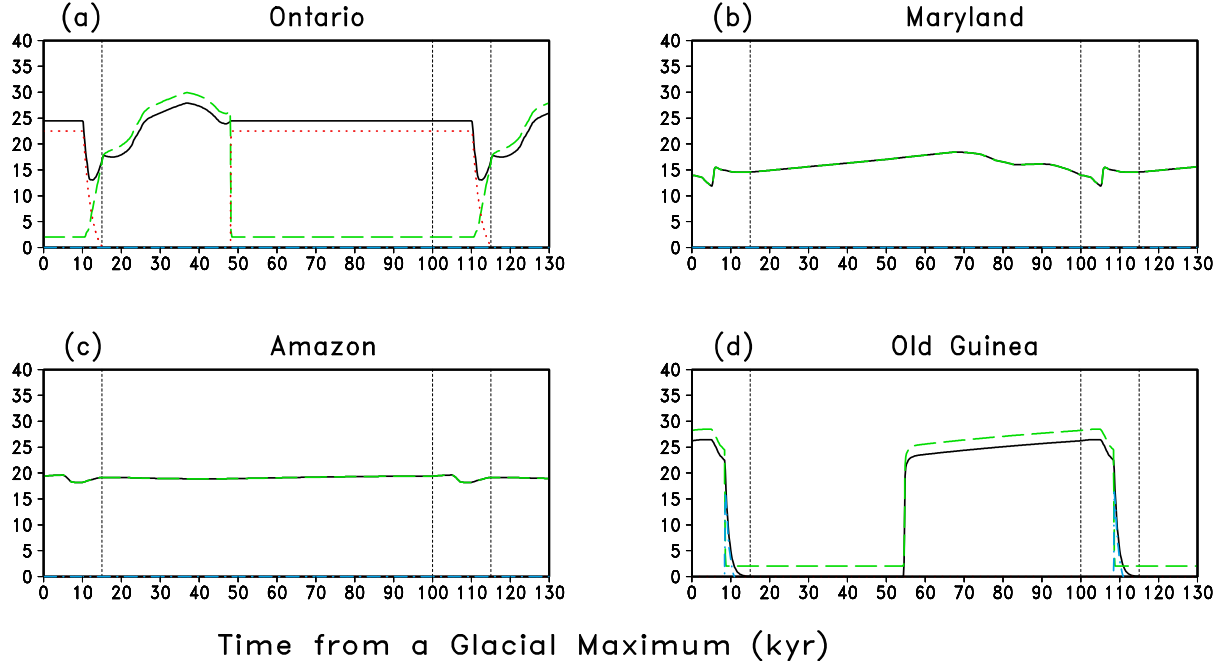


Fig. 6. Temporal evolution of carbon pools C_{land} , C_{b} , C_{bury} , and C_{subm} in kg m^{-2} at individual model grid points near: (a) Ontario (51°N , 91°W , buried under ice at glacial times); (b) Maryland (39°N , 77°W , in front of the Laurentide Ice Sheet); (c) Amazon (1°N , 64°W , tropical); (d) Old Guinea (11° , 139°E , continental shelf point submerged underwater at deglaciation). C_{land} is plotted in black, C_{b} in green, C_{bury} in red, and C_{subm} in blue. For clarity, C_{b} is shifted upward by 2 kg m^{-2} in (a) and (d); C_{bury} in (a) and C_{subm} in (d) are shifted downward by 2 kg m^{-2} . C_{land} and C_{b} overlap in (b) and (c) because they are identical.

on continental shelves, and C_{nois} is for the rest of the land (non-ice, non-shelf). This is different from partitioning by characteristic carbon pools whose coverage areas can vary in time (Eq. 1). At Gm, C_{ice} is 116 Gt larger, much less than the 381-Gt change in C_{bury} due to a partial cancellation from regrowth carbon assimilation. C_{nois} is larger at Gm by 198 Gt, corresponding to the overall enhanced carbon storage in these areas discussed above.

The land area is about $18 \times 10^6 \text{ m}^2$ larger at glacial maximum than interglacial as exposed continental shelves. This allows 254 Gt to grow on it at glacial maximum, and C_{shelf} is larger by 233 Gt at Gm than at Im. This shelf carbon C_{shelf} is part of the active biosphere C_{b} at Gm, and it is related to the other pools as:

$$C_{\text{b}} + C_{\text{subm}} = C_{\text{shelf}} + C_{\text{nonsshelf}}.$$

It is worth noting that none of the carbon pool differences in Table 2 is directly comparable to previous modeling studies which consider two equilibrium states with full vegetation and soil development at the Holocene, and do not include glacial burial carbon. A closer comparison is to take the difference of C_{b} in Fig. 4e between Gm and a post-interglacial period, e.g., at year 40 k which returns a value of about 100 Gt less at

Gm, a number within the range of these model results but on the low side.

Thus, the main reason for the difference of the present study and a number of past paleoecological and modeling estimates is that their estimates assume there is no carbon stored under ice. Moreover, the delayed regrowth relative to burial decomposition in our model renders the sign going in the opposite direction. In addition, the not so dry but much colder glacial climate allows more carbon to accumulate in soil without necessarily increasing above-ground biomass or changes in vegetation type. A process that acts in the other direction is the lowered plant productivity due to lower atmospheric CO_2 level which leads to less carbon at Gm. Uncertainties in the non-ice covered region aside, the ice-covered carbon needs to be included in any estimation of ice-age carbon storage on land.

The uncertainties with the most significant consequences include carbon in ice area C_{ice} , which can change up to 427 Gt (instead of the 116 Gt of the control simulation) at deglaciation if regrowth is much slower than burial carbon decomposition. If the glaciation process is such that some continental shelf area rises above sea level before being buried under ice such

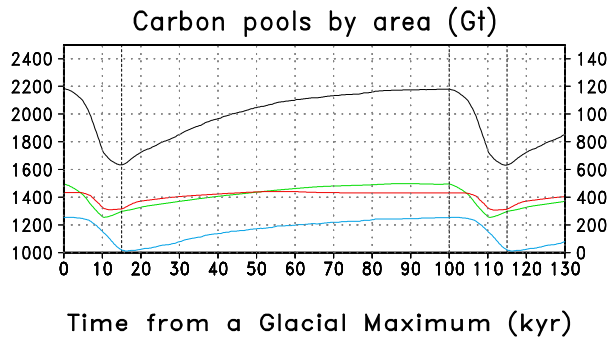


Fig. 7. Land carbon partitioned by characteristic areas that are constant in time: total C_{land} in black, carbon in non-ice/non-shelf area C_{nois} in green (labeled on the left), carbon in the area with changing ice C_{ice} in red, carbon on continental shelves C_{shelf} in blue (labeled on the right). C_{ice} changes by only 116 Gt from Gm to Im because regrowth partially cancels glacial burial carbon release.

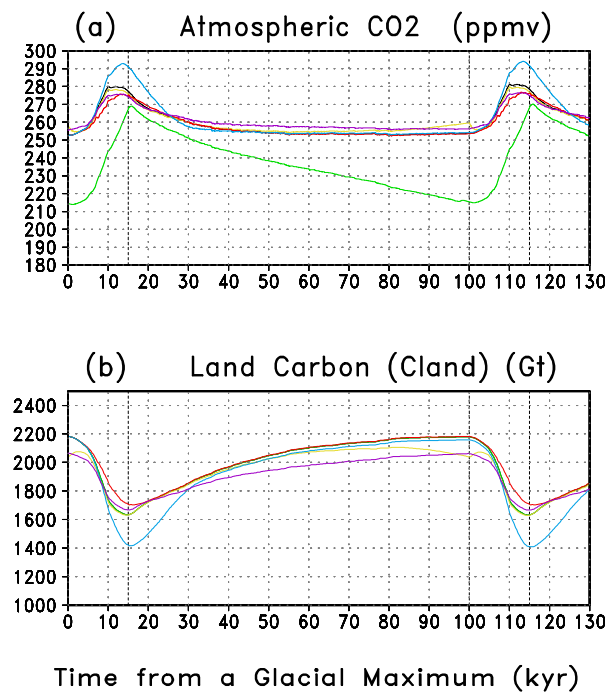


Fig. 8. Modeled atmospheric CO_2 (a) and land carbon storage (b) from the control run and 5 sensitivity experiments described in the text: control is in black line, SST4 in green, $\text{CO}_2\text{v}120$ in yellow, SoilD5h in red, SoilD20k in blue, and WarmGlac in purple. The largest change of a 55 ppmv deglacial CO_2 increase is due to a cooler glacial ocean in addition to the land carbon release (green) and a 40 ppmv increase due to a long delayed regrowth (blue).

as the Hudson Bay, additional carbon would accumulate there (not allowed in the current model). The burial pool would have been further increased if peatland is included (Klinger, 1991; Franzen, 1994; not

modeled explicitly here), although it is not clear how much peat carbon was available for burial at shorter interglacials such as the Holsteinian since present northern peatlands have accumulated mostly during the Holocene (Harden et al., 1992). On the other hand, the non-ice/non-shelf area carbon C_{nois} has a 198-Gt larger storage at Gm, which can be sensitive to the climate forcing and model parameterizations. For instance, the CCM1 climate used here has a colder glacial temperature (presumably more realistic) compared to an earlier version and some other models (Kutzbach et al., 1998; Pinot et al., 1999). Some of these uncertainties are assessed below using model sensitivity experiments.

6. Sensitivities

The assessment of uncertainties is difficult because of our limited knowledge of the wide range of processes involved, such as the glaciation history of burial carbon, and the relative timing of burial decomposition and regrowth. To explore a broad range of possibilities, the following five sensitivity experiments are conducted and the simulated atmospheric CO_2 and land carbon are summarized in Fig. 8 and Table 3. The simulation discussed above is referred to as the control run.

(1) Experiment SST4: sea surface temperature (SST) was set to 4°C lower everywhere at Gm than at Im, with interpolation from Im to Gm and a 1000-year delay to mimic the deep ocean response. Other ocean forcings are interglacial as in the control run.

(2) $\text{CO}_2\text{v}120$: CO_2 in vegetation photosynthesis varies between 280 to 120 (280-200 in the control run) ppmv, thus more than doubling the sensitivity to CO_2 effect due to the nonlinearity at low CO_2 level.

(3) SoilD5h: regrowth delay due to soil development after glacial retreat is 500 years at maximum (5000 years in control run).

(4) SoilD20k: regrowth delay is 20 000 years.

(5) WarmGlac: land temperature forcing at Gm is set at halfway between the CCM1's Gm and Im values, that is, only half as cold. This experiment tests both the model's sensitivity to differing climate forcing, and to the temperature dependence of vegetation and soil respiration rate.

The very rapid regrowth in SoilD5h only reduced the land carbon change by 72 Gt compared to the control run. The sensitivity to photosynthesis CO_2 and warmer glacial temperature is higher, both producing about 150 Gt less change in land carbon storage and only about 20 ppmv increase in atmospheric CO_2 .

Table 3. Land carbon storage (C_{land} ; in Gt) difference between glacial maximum and interglacial (Gm–Im) for the control run and 5 sensitivity runs described in the text

Control/SST4	CO ₂ v120	SoilD5h	SoilD20k	WarmGlac
547	407	475	749	395

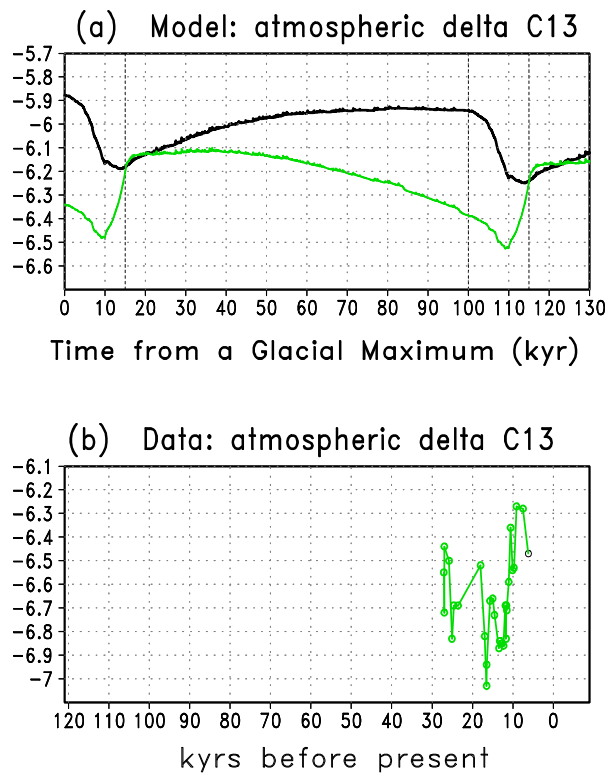


Fig. 9. (a) Atmospheric $\delta^{13}\text{C}$ (per thousand) simulated by the model, from the control run land+passive ocean scenario (black line), and a scenario with a 4°C SST cooling at glacial maximum (green line); (b) Atmospheric $\delta^{13}\text{C}$ measured from air trapped in ice core at Taylor Dome, Antarctica (Smith et al. 1999). In the land+cooler SST scenario, the input of light isotope enriched terrestrial carbon at deglaciation causes atmospheric $\delta^{13}\text{C}$ to drop initially, followed by rapid rise toward a high interglacial value in response to oceanic warming and regrowth on land.

In the other direction, the largest difference is made by the SST cooling: the atmospheric CO_2 change from glacial to interglacial is now 55 ppmv, compared to 30 ppmv in the control run. It is thus likely that the well-studied oceanic processes can account for the remaining difference in the observed CO_2 .

Also important is the longer regrowth delay in SoilD20k, which allows the glacial burial carbon to completely decompose before vegetation reclaims the formerly ice covered land. This leads to a 749-Gt release of land carbon at deglaciation, and a 40-ppmv increase in the atmospheric CO_2 . Thus, a combined

scenario of 4°C cooler SST and fast burial carbon decomposition relative to regrowth would generate about a 65-ppmv change in CO_2 .

7. Carbon-13

An important prediction of the current theory is that the atmospheric concentration of the rare isotope ^{13}C would decrease initially at deglaciation, in response to the release of the ^{13}C -depleted glacial burial carbon, which is derived from plants whose photosynthesis discriminates against the heavier isotope ^{13}C .

Figure 9a shows the model simulated atmospheric $\delta^{13}\text{C}$. In the control run where only contribution from terrestrial carbon change is considered, $\delta^{13}\text{C}$ increases slowly throughout glaciation because the assimilation of light carbon onto the land reservoir leaves the heavy isotope in the atmosphere. It then drops at deglaciation by about 0.3‰ from Gm to Im, before rising slowly back to its glacial value, because now regrowth outweighs the decomposition of burial carbon.

When SST is allowed to cool at glacial times (by 4°C at Gm; SST4), the modeled $\delta^{13}\text{C}$ shows more complicated features because of the opposite effects of ocean temperature and land carbon flux. The early stage of glaciation has a modest increase in $\delta^{13}\text{C}$ as land assimilates light carbon, but $\delta^{13}\text{C}$ starts to decline from a post-interglacial time (year 35 kyr) in response to the lowering of ocean temperature which now dominates the ^{13}C enrichment due to land carbon assimilation. At deglaciation, $\delta^{13}\text{C}$ drops until about 10 kyr into deglaciation (year 110 kyr) as the light glacial burial carbon is released, followed by rapid rise in response to ocean warming. The change in $\delta^{13}\text{C}$ from the deglaciation minimum to post-interglacial maximum is about 0.35‰. This change depends not only on the magnitude, but also on the relative timing of land carbon release and changes in the ocean. There is a slight overall decrease because the ocean ^{13}C has a timescale longer than 100 kyr so that ^{13}C has not reached complete equilibrium after the model's interglacial spinup period. It is likely that this long timescale has left its signature in observations.

Observational verification of ^{13}C change is hampered by a focus on mean glacial and interglacial values in most analyses and the difficulties in ice core $\delta^{13}\text{C}$ measurements (Leuenberger et al., 1992). Earlier measurements on ancient plants stowed away by

packrats showed a deglacial drop but with only two data points (Marino et al., 1992). Recent ice core data with improved temporal resolution appear to support a drop-rise transition at deglaciation (Fig. 9b; Smith et al., 1999).

It is speculated that a terrestrial carbon source at deglaciation would have also left its signature in the $\delta^{13}\text{C}$ record in the surface ocean which exchanges fluxes rapidly with the atmosphere. This would be consistent with a deglacial negative excursion observed in the surface and intermediate waters across the Pacific, Indian, and the tropical Atlantic oceans (Ninnemann and Charles, 1997; Spero and Lea, 2002). But the different behaviors in the North Atlantic and the deep waters suggest important regional differences likely due to changes in the thermohaline circulation and regional-scale nutrient loading (Keir, 1995; Lynch-Stieglitz and Fairbanks, 1994; Ninnemann and Charles, 1997). Thus, ice core $\delta^{13}\text{C}$ measurement offers a stringent constraint because it is a measure of the whole atmosphere. The results also suggest the strong need for further examination of the temporal and spatial characteristics of the isotope signals in the ocean.

8. Discussion and conclusions

It is demonstrated in a coupled atmosphere-land-ocean carbon model that the terrestrial biosphere alone can contribute about 30 ppmv, a significant fraction of the observed atmospheric CO_2 increase from glacial maximum to interglacial, corresponding to a transfer of 547 Gt of carbon from land to the atmosphere and ocean. This is caused mainly by the burial of vegetation and soil carbon at glaciation and its subsequent release at deglaciation, with additional contribution from the continental shelf and other areas. Together with other mechanisms in the ocean, the glacial burial hypothesis has the potential to provide a full answer to the glacial CO_2 problem.

The finding that land has larger carbon storage at a glacial maximum (thus a source of carbon at deglaciation) is different from most other estimates for three major reasons: 1) the inclusion of about 500 Gt of carbon buried under the ice sheets (the glacial burial hypothesis); 2) the delayed regrowth in the formerly ice covered regions (the importance of transient consideration, together with the multiple timescales in the ocean and sediments); 3) more carbon storage in non-ice covered regions due to the reduced decomposition rate of soil carbon at lowered temperature, which outcompetes the more modest effects of reduced precipitation and CO_2 fertilization. This last difference compared to other models is not large because similar

assumptions (i.e., equilibrium simulation with boreal landscape fully developed and without burial carbon) would lead to about 100 Gt less carbon at glacial maximum, a value within the range of other models but on the low side (Table 1). The first two effects were not included in previous studies. A combination of these effects at deglaciation leads to a 500-Gt land carbon release rather than the typical estimate of 500 Gt uptake.

The release of isotopically light terrestrial carbon initially drives down the atmospheric $\delta^{13}\text{C}$ which then rises due to regrowth on land and warming in the oceans. This drop-rise transition is consistent with the recent ice core measurements of $\delta^{13}\text{C}$ at the last deglaciation. The wide spread deglacial surface ocean $\delta^{13}\text{C}$ minimum is hypothesized to be a direct response to the atmospheric $\delta^{13}\text{C}$ change. The author has not attempted to come up with a coherent picture that is consistent with both the new land scenario and the spatiotemporally varying behavior of the full spectrum of surface and bottom foraminiferal $\delta^{13}\text{C}$ records.

However, many of the processes are not well known and some model parameterizations are not constrained well enough by our present knowledge. Nonetheless, the results reported here highlight the critical importance of considering the time dependent changes both on land and in the ocean, in particular, the accumulation of vegetation and soil carbon during regrowth after ice sheet retreat and its subsequent burial and release, as well as the multiple time scales in ocean circulation and sediment chemistry. The author therefore suggests a few key steps that can further advance our understanding of this problem:

- Search of direct evidence of glacial burial carbon under the former ice sheets such as the Laurentide, by discovering and analyzing the remains of a largely destroyed carbon reservoir.
- High resolution measurement of atmospheric carbon-13 preserved in ice cores, extending back in time to cover earlier deglaciations, because this provides critical information on the relative contributions of land and ocean.
- Transient coupling to high resolution ocean models with a sediment component, and incorporating other oceanic mechanisms, so as to compare with the vast array of ocean sediment data for both carbon and carbon-13; both whole ocean or basin wide synthesis and site-by-site comparison (forward method; Heinze, 2001) are needed.
- Intercomparison and validation of terrestrial carbon models and paleoclimate reconstructions, in order

to narrow down the uncertainties associated with climate forcing and model parameterizations.

Acknowledgments. The author is thankful for discussions with A. Ganopolsky, A. Mariotti, B. Runnegar, G. McDonald, C. Heinze, M. Scholze, J. Jouzel, M. Leuenberger, D. Archer, J. Adams, J. Sarmiento, M. Heimann, P. Falkowski, J. Collatz, and M. Cane, comments from an anonymous reviewer, and the hospitality and computing support from the Max-Planck Institut für Meteorologie, Hamburg in 2000, and from the Italian National Agency for New Technologies, Energy and Environment (ENEA) during his summer visits in 2001–2002. The ocean carbon models were kindly provided by C. Heinze, E. Maier-Reimer, and A. Ridgwell. This research was supported by NSF grant ATM-0196210 and the Alexander von Humboldt Foundation.

APPENDIX

The terrestrial carbon model Vegetation-Global-Atmosphere-Soil (VEGAS) simulates the dynamics of vegetation growth and competition among different plant functional types (PFTs). It includes 4 PFTs: broadleaf tree, needleleaf tree, cold grass, and warm grass. The different photosynthetic pathways are distinguished for C3 (the first three PFTs above) and C4 (warm grass) plants. Photosynthesis is a function of light, temperature, soil moisture, and CO₂. Accompanying the vegetation dynamics is the full terrestrial carbon cycle starting from the allocation of the photosynthetic carbon into three vegetation carbon pools: leaf, root, and wood. After accounting for respiration, the biomass turnover from these three vegetation carbon pools cascades into a fast, an intermediate, and finally a slow soil pool. Temperature and moisture dependent decomposition of these carbon pools returns carbon back into the atmosphere, thus closing the terrestrial carbon cycle. A decreasing temperature dependence of respiration from fast to slow soil pools takes into account the effects of physical protection of organic carbon by soil particles below ground (Liski et al., 1999). The vegetation component is coupled to land and atmosphere through a soil moisture dependence of photosynthesis and evapotranspiration, as well as dependence on temperature, radiation, and atmospheric CO₂. The isotope carbon-13 is modeled by assuming a different carbon discrimination for C3 and C4 plants, thus providing a diagnostic quantity useful for distinguishing ocean and land sources and sinks of atmospheric CO₂. Competition between C3 and C4 grass is a function of temperature and CO₂ following Collatz et al., (1998).

The ocean carbon model SUE (Ridgwell, 2001) simulates both the ocean CO₂ mixing and CaCO₃ sediment dissolution processes, as well as carbon 13. The version used here consists of 16 horizontal regions covering the major oceanic subbasins and 8 layers in the vertical, forced by the fields of modern circulation, temperature, salinity, etc. The author has also conducted a number of runs including the control run using the full 3D Hamburg Ocean Carbon Cycle Model (HAMOCC; Heinze and Maier-Reimer, 1999), and the results are very similar in terms of simulated atmospheric CO₂. Thus all the sensitivity runs were conducted using SUE.

REFERENCES

- Adams, J. M., H. Faure, L. Faure-Denard, J. M. McGlade, and others, 1990: Increase in terrestrial carbon storage from the last glacial maximum to the present. *Nature*, **348**, 711–714.
- Adams, J. M. and H. Faure, 1998: A new estimate of changing carbon storage on land since the last glacial maximum, based on global land ecosystem reconstruction. *Global Planet. Change*, **17**, 3–24.
- Archer, D., A. Winguth, D. Lea, and N. Mahowald, 2000: What caused the glacial/interglacial atmospheric pCO₂ cycles? *Rev. Geophys.*, **38**, 159–189.
- Beerling, D. J., 1999: New estimates of carbon transfer to terrestrial ecosystems between the last glacial maximum and the Holocene. *Terra Nova*, **11**, 162–167.
- Berger, W. H., and E. Vincent, 1986: Deep-sea carbonates: Reading the carbon isotope signal. *Geol. Rundschau.*, **75**, 249–269.
- Bird, M. I., J. Lloyd, and G. D. Farquhar, 1994: Terrestrial carbon storage at the LGM. *Nature*, **371**, 566–566.
- Broecker, W. S., and G. M. Henderson, 1998: The sequence of events surrounding Termination II and their implications for the cause of glacial-interglacial CO₂ changes. *Paleoceanography*, **13**, 352–364.
- Collatz, G. J., J. A. Berry, and J. S. Clark, 1998: Effects of climate and atmospheric CO₂ partial pressure on the global distribution of C-4 grasses: Present, past, and future. *Oecologia*, **114**, 441–454.
- Crowley, T. J., 1995: Ice age terrestrial carbon changes revisited. *Global Biogeochem. Cycle*, **9**, 377–389.
- Curry, W. B., J.-C. Duplessy, L. D. Labeyrie, and N. J. Shackleton, 1988: Changes in the distribution of $\delta^{13}\text{C}$ of deep water CO₂ between the last glacial and the Holocene. *Paleoceanography*, **3**, 317–341.
- Duplessy, J. -C., N. J. Shackleton, R. J. Fairbanks, L. D. Labeyrie, D. Oppo, and N. Kallel, 1988: Deep water source variations during the last climatic cycle and their impact on the global deep water circulation. *Paleoceanography* **3**, 343–360.
- Esser, G., and M. Lautenschlager, 1994: Estimating the change of carbon in the terrestrial biosphere from 18 000 BP to present using a carbon cycle model. *Environ. Pollut.*, **83**, 45–53.
- Falkowski, P., R. J. Scholes, E. Boyle, and others, 2000: The global carbon cycle: A test of our knowledge of earth as a system. *Science*, **290**, 291–296.
- Field, C. B., 2001: Plant physiology of the “missing” carbon sink. *Plant Physiology*, **125**, 25–28.

- Francois, L. M., C. Delire, P. Warnant, and G. Munhoven, 1998: Modelling the glacial-interglacial changes in the continental biosphere. *Global Planet. Change*, **17**, 37–52.
- Franzen, L. G., 1994: Are wetlands the key to the ice-age cycle enigma. *Ambio*, **23**, 300–308.
- Friedlingstein, P., C. Delire, J. F. Muller, and J. C. Gerard, 1992: The climate induced variation of the continental biosphere: a model simulation of the last glacial maximum. *Geophys. Res. Lett.*, **19**, 897–900.
- Friedlingstein, P., K. C. Prentice, I. Y. Fung, J. G. John, and G. P. Brasseur, 1995: Carbon-biosphere-climate interaction in the last glacial maximum climate. *J. Geophys. Res.*, **100**, 7203–7221.
- Gildor, H., and E. Tziperman, 2001: Physical mechanisms behind biogeochemical glacial-interglacial CO₂ variations. *Geophys. Res. Lett.*, **28**(12), 2421–2424.
- Harden, J. W., E. T. Sundquist, R. F. Stallard, and R. K. Mark, 1992: Dynamics of soil carbon during deglaciation of the Laurentide Ice Sheet. *Science*, **258**, 1921–1924.
- Heinze, C., 2001: Towards the time dependent modeling of sediment core data on a global basis. *Geophys. Res. Lett.*, **28**, 4211–4214.
- Heinze, C., and E. Maier-Reimer, 1999: The Hamburg Oceanic Carbon Cycle Circulation Model Version “HAMOCC2s” for long time integrations. DKRZ Rep. 20, Ger. Clim. Comput. Cent., Hamburg.
- Kaplan J. O., I. C. Prentice, W. Knorr, and others, 2002: Modeling the dynamics of terrestrial carbon storage since the Last Glacial Maximum. *Geophys. Res. Lett.*, **29**(22), 2074.
- Keir, R. S., 1995: Is there a component of Pleistocene CO₂ change associated with carbonate dissolution cycles. *Paleoceanography*, **10**: 871–880.
- Klinger, L. F., 1991: Peatland formation and ice ages: A possible Gaian mechanism related to community succession. *Scientists on Gaia*, S. H. Schneider and P. J. Boston, Eds., MIT press, Cambridge, Mass, 247–255.
- Kutzbach, J., R. Gallimore, S. Harrison, P. Behling, and others, 1998: Climate and biome simulations for the past 21 000 years. *Quaternary Sci. Rev.*, **17**, 473–506.
- Leuenberger, M., U. Siegenthaler, and C. C. Langway, 1992: Carbon isotope composition of atmospheric CO₂ during the last ice-age from an Antarctic ice core. *Nature*, **357**, 488–490.
- Liski, J., H. Ilvesniemi, A. Makela, C. J. Westman, 1999: CO₂ emissions from soil in response to climatic warming are overestimated-The decomposition of old soil organic matter is tolerant of temperature. *Ambio*, **28**, 171–174.
- Lynch-Stieglitz, J., and R. G. Fairbanks, 1994: A conservative tracer for glacial ocean circulation from carbon isotope and palaeo-nutrient measurements in benthic foraminifera. *Nature*, **369**: 308–310.
- MacAyeal, D. R., 1993: BINGE/PURGE oscillations of the Laurentide Ice Sheet as a cause of the North Atlantic Heinrich events. *Paleoceanography*, **8**, 775–784.
- Marino, B. D., M. B. McElroy, R. J. Salawitch, and W. G. Spaulding, 1992: Glacial-to-interglacial variations in the carbon isotopic composition of atmospheric CO₂. *Nature*, **357**, 461–466.
- Martin, J. H., 1990: Glacial-interglacial CO₂ change: The iron hypothesis. *Paleoceanography*, **5**, 1–13.
- Maslin, M., and E. Thomas, 2003: Balancing the deglacial global carbon budget: The hydrate factor. *Quaternary Sci. Rev.*, **22**, 1729–1736.
- Maslin, M. A., J. Adams, E. Thomas, H. Faure, and R. Haines-Young, 1995: Estimating the carbon transfer between the ocean, atmosphere and the terrestrial biosphere since the last glacial maximum. *Terra Nova*, **7**, 358–366.
- New, M., M. Hulme, and P. Jones, 1999: Representing twentieth-century space-time climate variability. Part I: Development of a 1961–90 mean monthly terrestrial climatology. *J. Climate.*, **12**, 829–856.
- Ninnemann, U. S., and C. D. Charles, 1997: Regional differences in Quaternary Subantarctic nutrient cycling: Link to intermediate and deep water ventilation. *Paleoceanography*, **12**: 560–567.
- Olson, J. S., R. M. Garrels, R. A. Berner, T. V. Armentano, M. I. Dyer, and D. H. Yaalon, 1985: The natural carbon cycle. *Atmospheric Carbon Dioxide and the Global Carbon Cycle*, J. R. Trabalka, Ed., US DOE/ER0239, Washington D.C., section 8.3.2, 186–188.
- Otto, D., D. Rasse, J. Kaplan, and others, 2002: Biospheric carbon stocks reconstructed at the Last Glacial Maximum: Comparison between general circulation models using prescribed and computed sea surface temperatures. *Global Planet. Change*, **33**, 117–138.
- Peltier, W. R., 1994: Ice age paleotopography. *Science*, **265**, 195–201.
- Peng, C. H., J. Guiot, and E van Campo, 1995: Reconstruction of the past terrestrial carbon storage of the Northern Hemisphere from the Osnabrueck Biosphere Model and palaeodata. *Climate Research*, **5**, 107–118.
- Petit, J. R., J. Jouzel, D. Raynaud, N. I. Barkov, and others, 1999: Climate and atmospheric history of the past 420 000 years from the Vostok ice core, Antarctica. *Nature*, **399**, 429–436.
- Pinot, S., G. Ramstein, S. P. Harrison, I. C. Prentice, and others, 1999: Tropical paleoclimates at the Last Glacial Maximum: Comparison of Paleoclimate Modeling Intercomparison Project (PMIP) simulations and paleodata. *Climate Dyn.*, **15**, 857–874.
- Prentice, I. C., M. T. Sykes, M. Lautenschlager, S. P. Harrison, O. Denissenki, and P. J. Bartlein, 1993: Modeling the increase in terrestrial carbon storage after the last glacial maximum. *Global Ecol. Biogeog. Lett.*, **3**, 67–76.
- Prentice, K. C., and I. Y. Fung, 1990: The sensitivity of terrestrial carbon storage to climate change. *Nature*, **346**, 48–51.
- Ridgwell, A. J., 2001: Glacial-interglacial perturbations in the global carbon cycle. Ph. D. dissertation, Univ. of East Anglia at Norwich, UK. Available at <http://tracer.env.uea.ac.uk/e114/ridgwell.2001.pdf>
- Schlesinger, W. H., 1991: *Biogeochemistry: An Analysis of Global Change*. Academic Press, San Diego, CA, USA, 443pp.
- Shackleton, N. J., 1977: Carbon-13 in Uvigerina: Tropical rainforest history and the equatorial Pacific carbonate dissolution cycles. *The Fate of Fossil Fuel CO₂ in the Oceans*, N. R. Andersen and A. Malahoff, Eds., Plenum, New York, 401–428.
- Sigman, D. M., and E. A. Boyle, 2000: Glacial/interglacial variations in atmospheric carbon dioxide. *Nature*, **407**, 859–869.

- Smith, H. J., H. Fischer, M. Wahlen, D. Mastroianni, and others, 1999: Dual modes of the carbon cycle since the Last Glacial Maximum. *Nature*, **400**, 248–250.
- Spero, H. J., and D. W. Lea, 2002: The cause of carbon isotope minimum events on glacial terminations. *Science*, **296**, 522–525.
- Stephens, B. B., and R. F. Keeling, 2000: The influence of Antarctic sea ice on glacial-interglacial CO₂ variations. *Nature*, **404**, 171–174.
- Sundquist, E. T., 1993: The global carbon dioxide budget. *Science*, **259**, 934–941.
- van Campo, E., J. Guiot, and C. H. Peng, 1993: A data-based re-appraisal of the terrestrial carbon budget at the Last Glacial Maximum. *Global Planet. Change*, **8**, 189–201.